

Doping-induced magnetic and topological transitions in $Mn_2X_2Te_5$ (X = Bi, Sb) bilayers

Wei Chen(陈威), Chuhan Tang(唐楚涵), Chao-Fei Liu(刘超飞), and Mingxing Chen(陈明星)
Citatio: Chin. Phys. B, 2025, 34 (**9**): 097304. DOI: 10.1088/1674-1056/ade4af
http://cpb.iphy.ac.cn; http://iopscience.iop.org/cpb

What follows is a list of articles you may be interested in

Electronic structure and carrier mobility of BSb nanotubes

Lantian Xue(薛岚天), Chennan Song(宋晨楠), Miaomiao Jian(见苗苗), Qiang Xu(许强), Yuhao Fu(付钰豪), Pengyue Gao(高朋越), and Yu Xie(谢禹)
Chin. Phys. B, 2025, 34 (**3**): 037304. DOI: 10.1088/1674-1056/adacd3

Emergence of metal-semiconductor phase transition in MX_2(M = Ni, Pd, Pt; X = S, Se, Te) moiré superlattices

Jie Li(李杰), Rui-Zi Zhang(张瑞梓), Jinbo Pan(潘金波), Ping Chen(陈平), and Shixuan Du(杜世萱)
Chin. Phys. B, 2025, 34 (**3**): 037302. DOI: 10.1088/1674-1056/ada7d9

$GaInX_3$ (X = S, Se, Te): Ultra-low thermal conductivity and excellent thermoelectric performance

Zhi-Fu Duan(段志福), Chang-Hao Ding(丁长浩), Zhong-Ke Ding(丁中科), Wei-Hua Xiao(肖威华), Fang Xie(谢芳), Nan-Nan Luo(罗南南), Jiang Zeng(曾犟), Li-Ming Tang(唐黎明), and Ke-Qiu Chen(陈克求)
Chin. Phys. B, 2024, 33 (**8**): 087302. DOI: 10.1088/1674-1056/ad47e3

Intrinsic valley-polarized quantum anomalous Hall effect in a two-dimensional germanene/MnI_2 van der Waals heterostructure

Xiao-Jing Dong(董晓晶) and Chang-Wen Zhang(张昌文)
Chin. Phys. B, 2024, 33 (**7**): 077303. DOI: 10.1088/1674-1056/ad4bbd

Effect of strain on structure and electronic properties of monolayer C_4N_4

Hao Chen(陈昊), Ying Xu(徐瑛), Jia-Shi Zhao(赵家石), and Dan Zhou(周丹)
Chin. Phys. B, 2024, 33 (**5**): 057302. DOI: 10.1088/1674-1056/ad260c

---

RAPID COMMUNICATION

Doping-induced magnetic and topological transitions in $Mn_2X_2Te_5$ (X = Bi, Sb) bilayers

Wei Chen(陈威)[1], Chuhan Tang(唐楚涵)[1], Chao-Fei Liu(刘超飞)[2], and Mingxing Chen(陈明星)[1,3,4†]

[1] *Key Laboratory for Matter Microstructure and Function of Hunan Province, Key Laboratory of Low-Dimensional Quantum Structures and Quantum Control of Ministry of Education, School of Physics and Electronics, Hunan Normal University, Changsha* 410081, *China*

[2] *School of Science, Jiangxi University of Science and Technology, Ganzhou* 341000, *China*

[3] *Hunan Research Center of the Basic Discipline for Quantum Effects and Quantum Technologies, Changsha* 410081, *China*

[4] *State Key Laboratory of Powder Metallurgy, Central South University, Changsha* 410083, *China*

(Received 27 March 2025; revised manuscript received 28 May 2025; accepted manuscript online 16 June 2025)

We investigate the magnetic and topological properties of $Mn_2X_2Te_5$ (X = Bi, Sb) using first-principles calculations. We find that both $Mn_2Bi_2Te_5$ and $Mn_2Sb_2Te_5$ bilayers exhibit A-type antiferromagnetic order, which can be understood based on the Goodenough–Kanamori–Anderson rules. We further find that an appropriate hole doping can induce a transition from the A-type antiferromagnetic phase to the ferromagnetic phase in these systems, which also experience a transition from a normal insulator to a quantum anomalous Hall phase. Our study thus demonstrates that tunable magnetism and band topology can be achieved in $Mn_2X_2Te_5$, which may be utilized in the design of new functional electronic devices.

Keywords: two-dimensional (2D) ferromagnetism, first-principles calculations, band topology

PACS: 73.22.–f, 73.20.At, 75.70.Ak, 71.15.Mb

DOI: 10.1088/1674-1056/ade4af **CSTR:** 32038.14.CPB.ade4af

1. Introduction

Two-dimensional (2D) magnetic materials have attracted extensive attention in recent years due to novel electronic properties and promising application prospects.[1–5] A landmark achievement occurred in recent years when ferromagnetic monolayers CrI_3 and $Cr_2Ge_2Te_6$ were discovered.[6–8] Since then, a series of 2D layered magnetic materials have been theoretically predicted and experimentally confirmed. To date, many ways have been developed to tune the magnetism and the electronic properties of 2D magnetic materials, such as external electric fields,[9–11] electrostatic doping,[12–16] strains,[17–20] layer stacking,[21–24] and interface engineering.[25,26]

Recently, this family was expanded with the discovery of layered magnetic topological insulators,[27,28] which exhibit novel electronic properties and physical effects, such as the quantum anomalous Hall effect and the axion insulating state.[29–32] In these systems, magnetic phase transitions are often accompanied by topological phase transitions. In particular, $MnBi_2Te_4$ thin films exhibit thickness-dependent magnetic and topological properties, which have ferromagnetic (FM) interlayer couplings for the odd-numbered layers and antiferromagnetic (AFM) interlayer couplings for even-numbered layers.[33–36] By tuning the interlayer magnetic coupling (IMC), a variety of topological phenomena can be realized in this system.[37–39] As sister compounds of the Mn–Bi–Te family, $Mn_2Bi_2Te_5$ and $Mn_2Sb_2Te_5$ have naturally attracted research interest and have been successfully synthesized. They are found to have AFM interlayer couplings.[40,41] Unlike $MnBi_2Te_4$, the magnetism of $Mn_2Bi_2Te_5$ does not depend on the number of layers, but its topological properties are still closely related to the magnetic order state.[42,43] Therefore, it is of interest to explore the ways of tuning the magnetism and band topology of $Mn_2Bi_2Te_5$.

In this study, we investigate the magnetic and topological properties of bilayer $Mn_2X_2Te_5$ using first-principles calculations. We find that the magnetic ground state of undoped $Mn_2X_2Te_5$ bilayer can be understood using the Goodenough–Kanamori–Anderson (GKA) rules. We also analyze the magnetic interactions in the systems based on the Heisenberg model and then examine the effects of electrostatic doping on their magnetic and topological properties. We find that appropriate hole doping can induce an AFM-to-FM transition, which is accompanied by a phase transition from a topologically trivial to a nontrivial state.

2. Computational methods

First-principles density functional theory (DFT) calculations were performed using the Vienna *ab initio* simulation package (VASP),[44,45] which uses the projector augmented wave method[46] to construct the pseudopotential, and the electron exchange–correlation functional was parametrized

†Corresponding author. E-mail: mxchen@hunnu.edu.cn

© 2025 Chinese Physical Society and IOP Publishing Ltd. All rights, including for text and data mining, AI training, and similar technologies, are reserved.

using the Perdew–Burke–Ernzerhof (PBE) functional.[47] The generalized gradient approximation (GGA+U) method was employed to describe the localized d orbitals of Mn atoms, with an effective Hubbard parameter $U_{\rm eff} = 3.0$ eV, consistent with previous studies.[42] The plane-wave basis with an energy cutoff of 400 eV was employed. The convergence criteria for the forces on each atom were set to 0.01 eV/Å, and the energy convergence criterion was set to 10^{-6} eV for structural relaxation. An $18 \times 18 \times 1$ Γ-centered k-mesh was used for self-consistent calculations. The vacuum space between adjacent slabs was set to be 20 Å. The DFT-D3 method with zero damping was used to treat the vdW interaction correction.[48] The Heisenberg spin model is used to describe the magnetic exchange interaction, which is derived by energy mapping.[49] Tight-binding models based on maximally localized Wannier functions were constructed by the Wannier90 code,[50] and the topological electronic structures were subsequently studied using the WannierTools package.[51]

3. Results and discussion

3.1. Structural properties of $Mn_2X_2Te_5$ bilayer

As shown in Fig. 1(a), the $Mn_2X_2Te_5$ compounds exhibit a layered rhombohedral structure with the space group P-3m1 (No. 164) and possess inversion symmetry. The unit cell of $Mn_2X_2Te_5$ consists of Te–X–Te–Mn–Te–Mn–Te–X–Te nonuple layers (NLs), as shown in Fig. 1(b), where the in-plane lattice constants a and b are 4.29 Å. Adjacent NLs are bound by van der Waals interactions, enabling the isolation of a single NL through mechanical exfoliation. Within the NL of $Mn_2X_2Te_5$, the $(MnTe)_2$ unit adopts a NaCl-like structure. The primitive cell of the $Mn_2X_2Te_5$ monolayer contains two Mn atoms, with six Te atoms coordinated around each Mn atom to form a distorted octahedron. These octahedra share edges along the z-direction, forming a continuous octahedral network. For clarity, a system with two stacked NLs is referred to as a $Mn_2X_2Te_5$ bilayer.

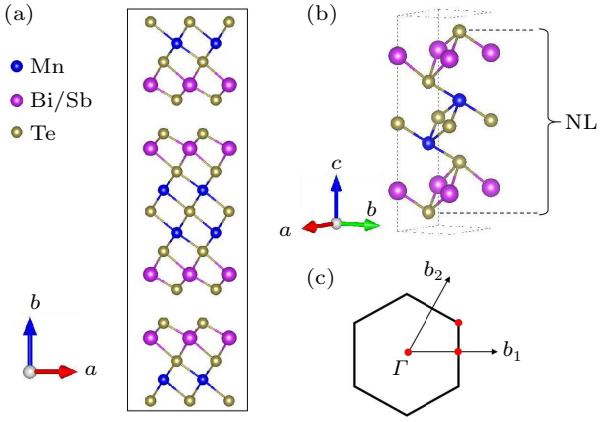


Fig. 1. Geometric structure of $Mn_2X_2Te_5$. (a) Side view of the geometric structure of the bulk phase, which contains two NLs. (b) Perspective view of an NL layer, i.e., a $Mn_2X_2Te_5$ monolayer. (c) The Brillouin zone of the $Mn_2X_2Te_5$ monolayer.

3.2. Magnetic properties of $Mn_2X_2Te_5$ bilayers

Both the bulk phases of $Mn_2Bi_2Te_5$ and $Mn_2Sb_2Te_5$ exhibit the A-type AFM order (Fig. 2(a)), which is labeled as AFM-1. The magnetism of the materials mainly stems from $Mn^{2+}(3d^5)$ in the high spin state $S = 5/2$. The magnetic moments on the Mn atoms are about $4.46\mu_B$ for both systems. There are two Mn atomic layers within each NL, which are hereafter referred to as Mn1 and Mn2. The Mn atoms within each atomic layer form a ferromagnetic order, and their magnetic moments are oriented out-of-plane. The adjacent Mn atomic layers within a NL, i.e., Mn1 and Mn2, have an antiferromagnetic interlayer coupling. In addition, the adjacent NLs also have AFM interlayer magnetic couplings (IMCs) (see Fig. 2(a)). In our calculations, in addition to the A-type AFM order, three additional magnetic configurations were considered, namely the ferromagnetic (FM) order and two other AFM states (AFM-2 and AFM-3) (see Figs. 2(c) and 2(d)). We use "u" ("d") to denote the direction of the magnetic moments on the Mn atoms. Among them, AFM-3 has a stripy in-plane AFM order (Fig. 2(d)).

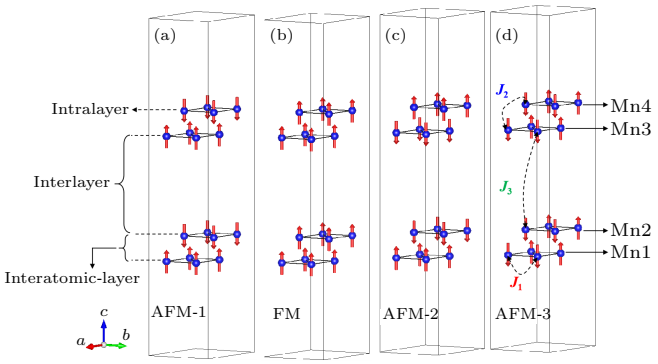


Fig. 2. Magnetic structures of $Mn_2X_2Te_5$ bilayer. (a)–(d) FM (uu_uu), AFM-1 (ud_ud) configuration, AFM-2 (ud_du), and AFM-3 (stripy) configurations, respectively. There are two Mn atomic layers within each NL. The blue balls represent the Mn atoms, whose magnetizations are shown by the red arrows and represented by u and d. J_n refers to the nth neighbor coupling constant.

Table 1. Energy differences between the three AFM and FM configurations for $Mn_2X_2Te_5$. A $2 \times 2 \times 1$ supercell is used for the calculation. The energy differences (ΔE) are in the unit of eV per formula cell (f.u.), which is calculated by $E_{\rm FM} - E_{\rm AFM}$ with $E_{\rm AFM}$ and $E_{\rm FM}$ representing the energies of the AFM and FM configurations, respectively.

Materials	Spin configuration	Magnetism	ΔE (meV/f.u.)
$Mn_2Bi_2Te_5$	↑↑ / ↑↑ (uu_uu)	FM	0
	↑↓ / ↑↓ (ud_ud)	AFM-1	−7.3
	↑↓ / ↓↑ (ud_du)	AFM-2	−6.9
	stripy-AFM (in-plane)	AFM-3	−0.5
$Mn_2Sb_2Te_5$	↑↑ / ↑↑ (uu_uu)	FM	0
	↑↓ / ↑↓ (ud_ud)	AFM-1	−1.2
	↑↓ / ↓↑ (ud_du)	AFM-2	−0.6
	stripy-AFM (in-plane)	AFM-3	7.3

To assess the relative stability of different magnetic orders, the energies of the AFM configurations are compared with that of the FM state. As summarized in Table 1, the three

AFM states exhibit lower energies than the FM state. Specifically, the AFM-1 state has the lowest energy, with $Mn_2Bi_2Te_5$ and $Mn_2Sb_2Te_5$ displaying energy reductions of 7.3 meV/f.u. and 1.2 meV/f.u. relative to the FM counterparts, respectively. Therefore, the magnetic ground state of $Mn_2X_2Te_5$ bilayers is AFM-1, which is consistent with previous studies.[42] In addition, we have investigated the stability using different functionals for the interlayer vdW interactions, which all show the same trend.

We calculated the magnetic exchange constants J to gain insight into the magnetic interactions. In order to consider the in-plane antiferromagnetic configuration (AFM-3), we used a $2\times2\times1$ supercell for the calculations. Then, we mapped the total energy of different magnetic configurations to the Heisenberg spin Hamiltonian.

$$H = E_0 - \sum_{ij} J_1 S_i S_j - \sum_{ij} J_2 S_i S_j - \sum_{ij} J_3 S_i S_j, \tag{1}$$

where E_0 is a constant independent of the magnetic order, S_i and S_j are the spin angular momentum on lattice sites i and j, respectively, and $S_{i,j}$ are normalized (i.e., $|S_{i,j}| = 1$). In Eq. (1), J_1, J_2 and J_3 represent the exchange coupling parameters between the nearest neighbors of Mn atoms within the Mn atomic layer, the nearest neighbors between Mn atoms in different atomic layers within an NL, and the nearest neighbors of Mn atoms between adjacent NLs, respectively (Fig. 2(d)). The corresponding energy expressions for the four magnetic configurations can be written as

$$E_{\mathrm{FM}} = E - 48J_1 - 24J_2 - 12J_3, \tag{2}$$

$$E_{\mathrm{AFM\text{-}1}} = E - 48J_1 + 24J_2 + 12J_3, \tag{3}$$

$$E_{\mathrm{AFM\text{-}2}} = E - 48J_1 + 24J_2 - 12J_3, \tag{4}$$

$$E_{\mathrm{AFM\text{-}3}} = E + 16J_1 - 18J_2 - 4J_3. \tag{5}$$

From the above equations, the spin exchange parameters J_1, J_2, and J_3 can be calculated and are summarized in Table 2. Since the Mn2–Mn3 distance is larger than that of the nearest Mn1–Mn2 and Mn1–Mn3 pairs, the amplitude of $|J_3|$ is much smaller than $|J_1|$. The J_1 of $Mn_2Bi_2Te_5$ and $Mn_2Sb_2Te_5$ is positive, while J_2 and J_3 are negative, indicating that the intralayer magnetic coupling within the Mn atomic layer tends to be ferromagnetic, whereas the Mn atoms in different atomic layers tend to couple antiferromagnetically.

Table 2. Exchange interaction parameters J_n for $Mn_2X_2Te_5$ bilayers. The atomic distance corresponding to the coupling between neighboring Mn atoms are also given.

Material	$2\times2\times1$ 2 NL $Mn_2Bi_2Te_5$		$2\times2\times1$ 2 NL $Mn_2Sb_2Te_5$	
J_n	Distance (Å)	Value (meV/f.u.)	Distance (Å)	Value (meV/f.u.)
J_1	4.31	0.03	4.26	0.12
J_2	4.17	−0.144	4.22	−0.012
J_3	14.24	−0.017	14.06	−0.025

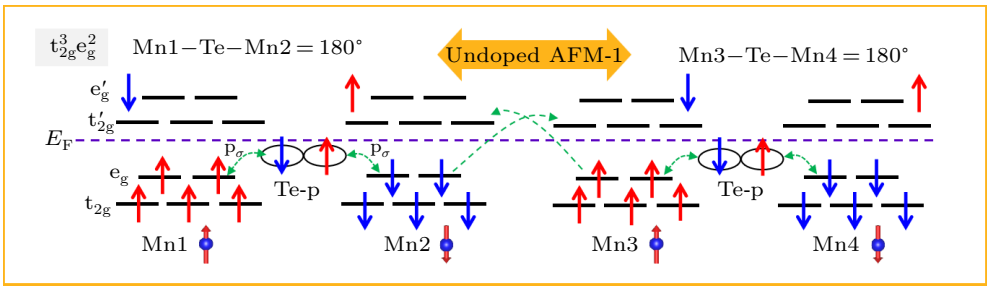


Fig. 3. Schematic diagram of possible exchange paths for $Mn_2X_2Te_5$ bilayer in the AFM-1 state. The five 3d electrons of the Mn^{2+} ion fully occupy the majority states. The red arrows and blue arrows represent up and down spins, respectively. The green curves with an arrow indicate electron hopping between neighboring Mn ions. The purple dotted line indicates the Fermi level, and t_{2g}' and e_g' indicate the d orbitals above the Fermi level in an unoccupied state.

In addition, the intralayer magnetic interactions (i.e., J_1 and J_2) in $Mn_2X_2Te_5$ can be further understood using the semi-empirical GKA rules. The d^5 orbital of Mn^{2+} is split into triply degenerate t_{2g} (d_{xy}, d_{yz}, d_{zx}) and doubly degenerate e_g ($d_{x^2-y^2}$, d_{z^2}) orbitals under the effect of the distorted octahedral crystal field. The 3d electrons of Mn^{2+} form a high spin state (t_{2g} and e_g are both half occupied states) as shown in Fig. 3. The superexchange interaction between neighboring Mn ions within each Mn atomic layer (J_1) is mainly associated with the overlap of the d orbital of Mn and the p orbital of Te. According to the GKA 3rd rule, when the d orbital of the cation is half-filled and the cation–anion–cation bond angle is about 90°, FM coupling is favored. In our case, the Mn–Te–Mn bond angle within the Mn atomic layer is approximately 90°. Therefore, the Mn(1)–Te–Mn(1) superexchange interaction appears to be FM, i.e., $J_1 > 0$. In addition, according to the GKA 1st rule, when the cation d orbital is half-filled and the cation–anion–cation bond angle is about 180°, the superexchange interaction tends to be AFM. The Mn1–Te–Mn2 bond angle within a NL is close to 180°. So Mn1 and Mn2 have an AFM coupling, i.e., $J_2 < 0$.

By inspecting the geometric structure, one can see that there are two $BiTe_2$ units and a vdw gap between Mn2 and Mn3 atoms. This situation makes the IMCs (i.e., J_3) much

weaker and more complicated than the intralayer ones. Therefore, the GKA rules are no longer applicable to the IMCs. Instead, we understand them by a model previously proposed for $MnBi_2Te_4$ bilayer and other 2D magnetic bilayers.[26,52] This model finds that the sign of the IMCs is related to the occupation of the d-orbitals of the magnetic ions. Since the Mn^{2+} ion is half-filled, i.e., the majority states of the Mn-t_{2g} and e_g orbitals are fully occupied by five d electrons, the IMC has to be AFM (i.e., $J_3 < 0$) so that there is a hopping channel between the occupied Mn-t_{2g} and the empty Mn–$t_{2g'}$ orbitals. In this case, the FM state is unfavorable since there are no hopping channels. Reducing the occupation of the Mn-3d orbitals favors the interlayer FM interactions.

3.3. Band structure and topological properties of $Mn_2X_2Te_5$ bilayers

We have calculated the band structure of the magnetic ground state (AFM-1 configuration) for $Mn_2X_2Te_5$ bilayers with and without spin–orbit coupling (SOC). As shown in Figs. 4(a) and 4(d), in the absence of SOC, the spin-up and spin-down bands are fully degenerate. The valence band maximum (VBM) is positioned at the Γ point, while the conduction band minimum (CBM) resides at the M point for both systems. To elucidate the orbital contributions, we plotted the orbital-projected band structure and projected density of states (PDOS). Figures 4(b) and 4(e) demonstrate that near the Fermi level, the Te p-orbitals dominate the valence band maximum, whereas the Bi p-orbitals primarily contribute to the conduction band edge.

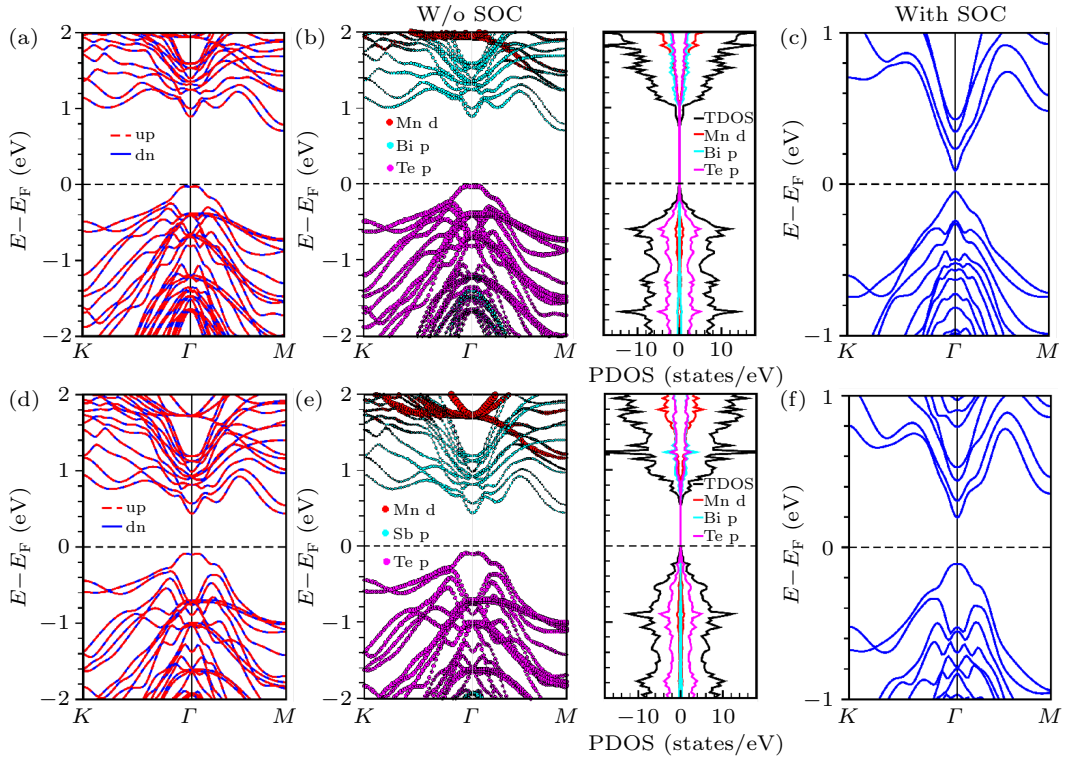


Fig. 4. Electronic structure of the AFM-1 state for $Mn_2X_2Te_5$ bilayers. (a) and (d) Band structures without SOC for $Mn_2Bi_2Te_5$ and $Mn_2Sb_2Te_5$ bilayers, respectively. (b) and (e) Atom-projected band structures and orbital-PDOS without SOC for corresponding compounds. (c) and (f) Band structures with SOC.

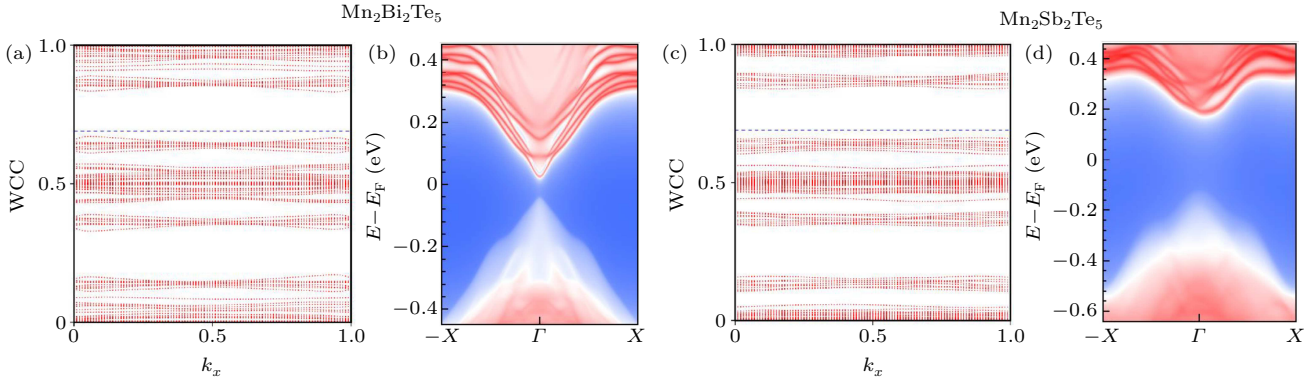


Fig. 5. Topological properties of the AFM-1 state for $Mn_2X_2Te_5$ bilayers. (a) and (c) The evolution of the WCC and (b) and (d) the corresponding edge states along (100). The upper panels are for $Mn_2Bi_2Te_5$ and the lower panels are for $Mn_2Sb_2Te_5$.

The Mn d-orbitals remain far from the Fermi level. This result is consistent with the PDOS plots, which indicate that the states near the Fermi level originate predominantly from Te and Bi/Sb. When SOC is included (Figs. 4(c) and 5(f)), the CBM shifts from the M point to the Γ point, giving rise to band gaps of about 0.13 eV and 0.30 eV for $Mn_2Bi_2Te_5$ and $Mn_2Sb_2Te_5$, respectively.

To study the topological properties of the system, we investigate the evolution of the Wannier charge center (WCC) for $Mn_2Bi_2Te_5$ and $Mn_2Sb_2Te_5$ bilayers, as shown in Figs. 5(a) and 5(c). As a result, we obtain $C = 0$ for both compounds. This result suggests that the AFM-1 state of $Mn_2X_2Te_5$ bilayers is a conventional insulator. Our result of $Mn_2Bi_2Te_5$ agrees with a previous study.[42] We further calculated the edge states for both compounds. The absence of gapless edge states in both systems suggests a topologically trivial nature.

3.4. Effect of hole doping

Carrier doping is a widely adopted strategy for modulating the magnetic properties of two-dimensional magnetic insulators. Based the mechanism of the AFM ground state discussed above, a reduced occupation in the e_g orbitals may lead to the FM order (Fig. 6(a)), which can be achieved by hole doping. To explore this effect in $Mn_2X_2Te_5$ bilayers, we performed spin-polarized calculations by introducing electrastatic hole doping. The relative stability of the three AFM states was evaluated by comparing their energies with the FM state. As shown in Figs. 6(b) and 6(d), one can see that the energy difference (ΔE) between the AFM-1 and FM states gradually increases with the increasing of the hole concentration, and transitioning from negative to positive. This trend signifies a magnetic phase transition from the AFM-1 ground state to the FM state at critical doping levels of 0.1 hole/f.u. for

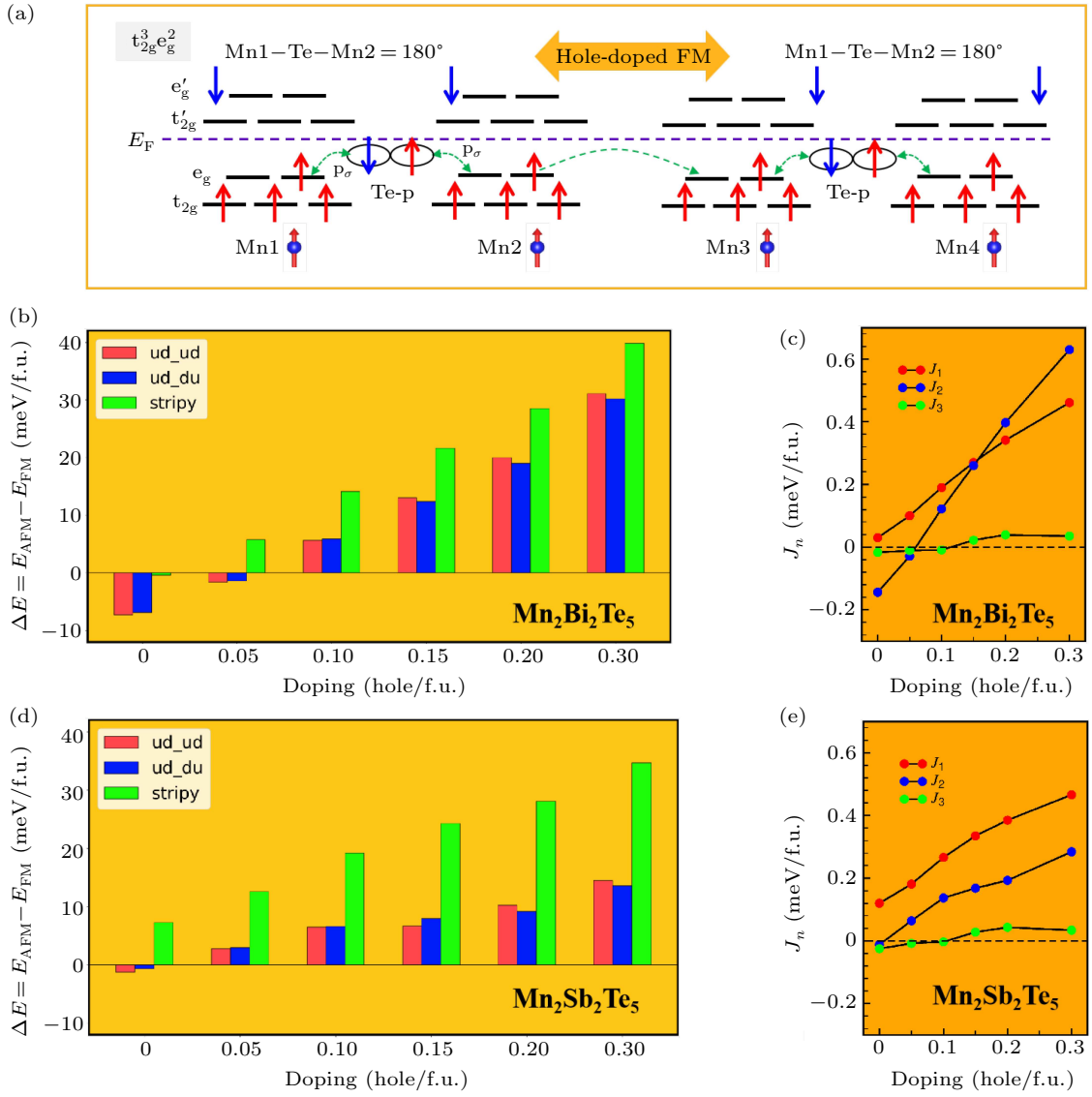


Fig. 6. The evolution of the magnetism of the $Mn_2X_2Te_5$ bilayer under hole doping. (a) The hopping channels for the FM state. (b) and (d) respectively show the energy difference between the FM state and AFM states as a function of doping concentration for the two systems. (c) and (e) respectively show the magnetic exchange parameters of $Mn_2Bi_2Te_5$ bilayer and $Mn_2Sb_2Te_5$ bilayer.

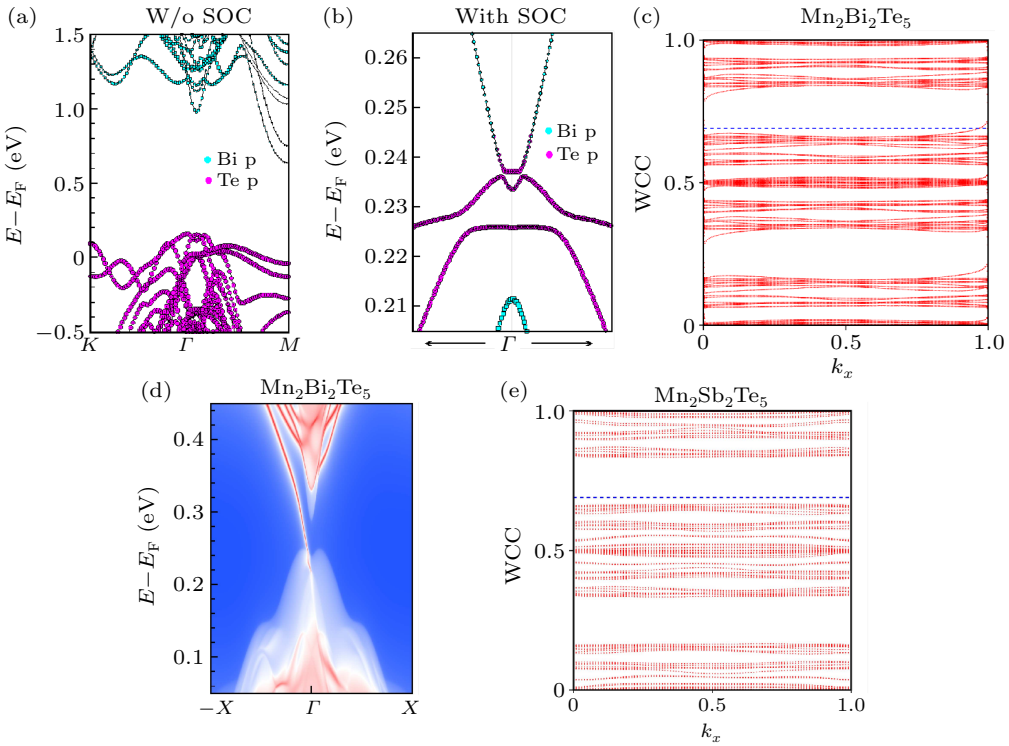


Fig. 7. Orbital-projected bands for the FM state of $Mn_2Bi_2Te_5$ bilayer with 0.2 hole/f.u. (a) and (b) show the orbital-projected bands for $Mn_2Bi_2Te_5$ without SOC and with SOC, respectively. (c) and (d) show the evolution of the WCC and the edge states, respectively. (e) When the hole concentration is 0.2 hole/f.u., the evolution of the Wannier charge center of the $Mn_2Sb_2Te_5$ bilayer ferromagnetic state is shown.

$Mn_2Bi_2Te_5$ and 0.05 hole/f.u. for $Mn_2Sb_2Te_5$. Similar to $MnBi_2Te_4$, electron doping can also lead to the AFM-to-FM transition,[26] the mechanism of which will not be discussed further.

In addition, we further analyzed the doping-dependent magnetic exchange parameters (Figs. 6(c) and 6(e)). The monotonic enhancement of exchange constants with hole doping directly suggests that the AFM IMC is weakened and the FM IMC is stabilized. This behavior is due to the reduced occupation of the d orbitals, which makes the $e_g\uparrow - \{p\cdots p\} - e_g\uparrow$ hopping channel energetically favorable, thus enhancing the stability of the FM IMCs. Meanwhile, hole doping reduces the number of d orbital electrons of Mn atoms, therefore slightly reducing the magnetic moment on Mn correspondingly. For instance, the magnetic moments are reduced by about $0.04\mu_B$.

The orbital-projected band structures without and with SOC effect for $Mn_2Bi_2Te_5$ are shown in Figs. 7(a) and 7(b). A comparison finds that the SOC effect induces a band inversion between the CBM and VBM at the Γ point. We calculated the Chern numbers for $Mn_2Bi_2Te_5$ bilayers and $Mn_2Sb_2Te_5$ bilayers in the ferromagnetic state at a doping concentration of 0.2 hole/f.u. For the $Mn_2Bi_2Te_5$ bilayer, gapless edge states appear (Fig. 7(c)). Moreover, one obtains $C = 1$ from the WCC plot shown in Fig. 7(d), suggesting its nontrivial topological properties. These results indicate that the quantum anomalous Hall phase can be realized in $Mn_2Bi_2Te_5$ via hole doping. In contrast, there is no band inversion for the $Mn_2Sb_2Te_5$ bilayer with inclusion of SOC (not shown) because it has a much larger band gap. Further calculations of WCC (Fig. 7(e)) and edge states again confirm that it remains topologically trivial.

4. Conclusion

In summary, we have systematically investigated the magnetic and electronic properties of $Mn_2X_2Te_5$ bilayers using first-principles calculations. Our results reveal that both $Mn_2Bi_2Te_5$ and $Mn_2Sb_2Te_5$ bilayers exhibit the A-type AFM ground state with conventional insulating behavior. We used the Heisenberg spin model to evaluate the magnetic exchange constants and applied the GKA rules to understand the magnetism. Then, we explored the effects of hole doping on the IMC and topological properties of these systems. Our results demonstrate that appropriate hole doping induces a transition in the magnetic ground state from A-type AFM to the FM state. In particular, for the $Mn_2Bi_2Te_5$ bilayer, the magnetic transition is accompanied by a topological phase transition, namely, it evolves from a conventional insulator into the QAH phase. In contrast, the $Mn_2Sb_2Te_5$ bilayer remains topologically trivial across the doping-induced magnetic transition.

Acknowledgments

Project supported by the National Natural Science Foundation of China (Grants Nos. 12174098 and 12574262), and the Major Fundamental Research Program of Hunan Province (Grants No. 2025ZYJ004), and the State Key Laboratory of

Powder Metallurgy, Central South University, China. Calculations were carried out in part using computing resources at the High-Performance Computing Platform of Hunan Normal University.

References

[1] Burch K S, Mandrus D and Park J G 2018 *Nature* **563** 47
[2] Kurebayashi H, Garcia J H, Khan S, Sinova J and Roche S 2022 *Nat. Rev. Phys.* **4** 150
[3] Li H, Ruan S and Zeng Y J 2019 *Adv. Mater.* **31** 1900065
[4] Wang Q H, Bedoya-Pinto A, Blei M, Dismukes A H, Hamo A, Jenkins S and Santos E J 2022 *ACS Nano* **16** 6960
[5] Ahn Y, Guo X, Son S, Sun Z and Zhao L 2024 *Prog. Quantum Electron.* **93** 100498
[6] Zhang W B, Qu Q, Zhu P and Lam C H 2015 *J. Mater. Chem. C* **3** 12457
[7] Gong C, Li L, Li Z, Ji H, Stern A, Xia Y and Zhang X 2017 *Nature* **546** 265
[8] Huang B, Clark G, Navarro-Moratalla E, Klein D R, Cheng R, Seyler K L and Xu X 2017 *Nature* **546** 270
[9] Huang B, Clark G, Klein D R, MacNeill D, Navarro-Moratalla E, Seyler K L and Xu X 2018 *Nat. Nanotechnol.* **13** 544
[10] Jiang S, Shan J and Mak K F 2018 *Nat. Mater.* **17** 406
[11] Wang Z, Zhang T, Ding M, Dong B, Li Y, Chen M and Zhang Z 2018 *Nat. Nanotechnol.* **13** 554
[12] Jiang S, Li L, Wang Z, Mak K F and Shan J 2018 *Nat. Nanotechnol.* **13** 549
[13] Tan C, Xie W Q, Zheng G, Aloufi N, Albarakati S, Algarni M and Wang L 2021 *Nano Lett.* **21** 5599
[14] Li X, Wu X and Yang J 2014 *J. Am. Chem. Soc.* **136** 11065
[15] Mi M, Zheng X, Wang S, Zhou Y, Yu L, Xiao H and Wang Y 2022 *Adv. Funct. Mater.* **32** 2112750
[16] Lu Y, Wang H, Wang L and Yang L 2022 *Phys. Rev. B* **106** 205403
[17] Qi Y, Sadi M A, Hu D, Zheng M, Wu Z, Jiang Y and Chen Y P 2023 *Adv. Mater.* **35** 2205714
[18] Cenker J, Sivakumar S, Xie K, Miller A, Thijssen P, Liu Z and Xu X 2022 *Nat. Nanotechnol.* **17** 256
[19] Webster L and Yan J A 2018 *Phys. Rev. B* **98** 144411
[20] Wang Y, Wang C, Liang S J, Ma Z, Xu K, Liu X and Miao F 2020 *Adv. Mater.* **32** 2004533
[21] Kong X, Yoon H, Han M J and Liang L 2021 *Nanoscale* **13** 16172
[22] Xun W, Wu C, Sun H, Zhang W, Wu Y Z and Li P 2024 *Nano Lett.* **24** 3541
[23] Yang S, Xu X, Han B, Gu P, Guzman R, Song Y and Ye Y 2023 *J. Am. Chem. Soc.* **145** 28184
[24] Chen W, Sun Z, Wang Z, Gu L, Xu X, Wu S and Gao C 2019 *Science* **366** 983
[25] Cheng H X, Zhou J, Wang C, Ji W and Zhang Y N 2021 *Phys. Rev. B* **104** 064443
[26] Yu G, Tang C, Tian Z, Zhu Z, Liu P, Pan A, Chen M and Chen X Q 2023 *Phys. Rev. B* **108** 014106
[27] Xu Y, Elcoro L, Song Z D, Wieder B J, Vergniory M G, Regnault N and Bernevig B A 2020 *Nature* **586** 702
[28] Zhang X, Wang X, He T, Wang L, Yu W W, Liu Y and Cheng Z 2023 *Sci. Bull.* **68** 2639
[29] Moore J E. 2010 *Nature* **464** 194
[30] Tokura Y, Yasuda K and Tsukazaki A 2019 *Nat. Rev. Phys.* **1** 126
[31] Yu R, Zhang W, Zhang H J, Zhang S C, Dai X and Fang Z 2010 *Science* **329** 61
[32] Bernevig B A, Felser C and Beidenkopf H 2022 *Nature* **603** 41
[33] Li J, Li Y, Du S, Wang Z, Gu B L, Zhang S C and Xu Y 2019 *Sci. Adv.* **5** eaaw5685
[34] Deng Y, Yu Y, Shi M Z, Guo Z, Xu Z, Wang J and Zhang Y 2020 *Science* **367** 895
[35] Otrokov M M, Rusinov I P, Blanco-Rey M, Hoffmann M, Vyazovskaya A Y, Eremeev S V and Chulkov E V 2019 *Phys. Rev. Lett.* **122** 107202
[36] He K 2020 *npj Quantum Mater.* **5** 90
[37] Zhao Y and Liu Q 2021 *Appl. Phys. Lett.* **119** 060502
[38] Liu C, Wang Y, Yang M, Mao J, Li H, Li Y and Wang Y 2021 *Nat. Commun.* **12** 4647
[39] Liu C, Wang Y, Li H, Wu Y, Li Y, Li J and Wang Y 2020 *Nat. Mater.* **19** 522
[40] Cao L, Han S, Lv Y Y, Wang D, Luo Y C, Zhang Y Y and Chen Y F 2021 *Phys. Rev. B* **104** 054421
[41] Saxena A and Awana V P S 2023 *J. Phys.: Condens. Matter* **36** 085704
[42] Li, Y, Jiang Y, Zhang J, Liu Z, Yang Z and Wang J 2020 *Phys. Rev. B* **102** 121107
[43] Eremeev S V, Otrokov M M, Ernst A and Chulkov E V 2022 *Phys. Rev. B* **105** 195105
[44] Kresse G and Furthmüller J 1996 *Phys. Rev. B* **54** 11169
[45] Kresse G and Furthmüller J 1996 *Comput. Mater. Sci.* **6** 15
[46] Kresse G and Joubert D 1999 *Phys. Rev. B* **59** 1758
[47] Perdew J P, Burke K and Ernzerhof M 1996 *Phys. Rev. Lett.* **77** 3865
[48] Grimme S, Antony J, Ehrlich S and Krieg H 2010 *J. Chem. Phys.* **132** 154104
[49] Xiang H, Lee C, Koo H J, Gong X and Whangbo M H 2012 *Dalton Trans.* **42** 823
[50] Pizzi G, Vitale V, Arita R, Blügel S, Freimuth F, Géranton G and Yates J R 2020 *J. Phys.: Condens. Matter* **32** 165902
[51] Wu Q, Zhang S, Song H F, Troyer M and Soluyanov A A 2018 *Comput. Phys. Commun.* **224** 405
[52] Li Z, Li J, He K, Wan X, Duan W and Xu Y 2020 *Phys. Rev. B* **102** 081107